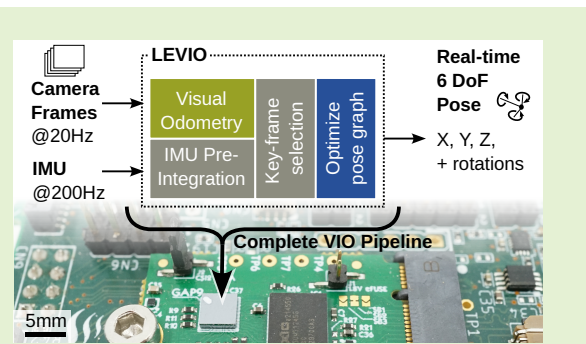


# LEVIO: Lightweight Embedded Visual Inertial Odometry for Resource-Constrained Devices

Jonas Kühne, *Member, IEEE*, Christian Vogt, *Member, IEEE*,  
 Michele Magno, *Senior Member, IEEE*, and Luca Benini, *Fellow, IEEE*

**Abstract**— Accurate, infrastructure-less sensor systems for motion tracking are essential for mobile robotics and augmented reality (AR) applications. The most popular state-of-the-art visual-inertial odometry (VIO) systems, however, are too computationally demanding for resource-constrained hardware, such as micro-drones and smart glasses. This work presents LEVIO, a fully featured VIO pipeline optimized for ultra-low-power compute platforms, allowing six-degrees-of-freedom (DoF) real-time sensing. LEVIO incorporates established VIO components such as Oriented FAST and Rotated BRIEF (ORB) feature tracking and bundle adjustment, while emphasizing a computationally efficient architecture with parallelization and low memory usage to suit embedded microcontrollers and low-power systems-on-chip (SoCs). The paper proposes and details the algorithmic design choices and the hardware-software co-optimization approach, and presents real-time performance on resource-constrained hardware. LEVIO is validated on a parallel-processing ultra-low-power RISC-V SoC, achieving 20 FPS while consuming less than 100 mW, and benchmarked against public VIO datasets, offering a compelling balance between efficiency and accuracy. To facilitate reproducibility and adoption, the complete implementation is released as open-source.

**Index Terms**— Constrained Devices, Embedded Devices, Energy Efficient Devices, Cyber-Physical Systems



## I. INTRODUCTION

In robotic and augmented reality tasks, tracking the device's movement relative to its surroundings is essential [1]. While infrastructure-based indoor position sensing can either be achieved with cost intensive high performance setups (e.g., motion tracking [2]), or at a lower accuracy and cost (e.g., radio localization with Wi-Fi [1], [3] or ultra-wide-band anchors [4]) the resulting infrastructure restricts the tracking to a defined area and generates additional recurring costs of infrastructure maintenance. To enable truly autonomous operation in robotics, both indoors and outdoors, and full freedom of movement for augmented reality tasks, future movement tracking needs to be infrastructure-less and accurate [5].

Infrastructure-less position-tracking systems are an established research field, mostly focusing on camera sensors in combination with Visual Odometry (VO) algorithms [6]. This

Jonas Kühne is with the Integrated Systems Laboratory and the Center for Project-Based Learning, ETH Zurich, 8092 Zurich, Switzerland (e-mail: kuehnej@ethz.ch).

Christian Vogt is with the Center for Project-Based Learning, ETH Zurich, 8092 Zurich, Switzerland (e-mail: christian.vogt@pbl.ee.ethz.ch).

Michele Magno is with the Center for Project-Based Learning, ETH Zurich, 8092 Zurich, Switzerland (e-mail: michele.magno@pbl.ee.ethz.ch).

Luca Benini is with the Integrated Systems Laboratory, ETH Zurich, 8092 Zurich, Switzerland, and also with the Department of Electrical, Electronic and Information Engineering, University of Bologna, 40136 Bologna, Italy (e-mail: luca.benini@unibo.it).

is a practical approach [7], thanks to the wide availability and affordability of small and low-power camera modules. VO algorithms are often augmented with Inertial Measurement Unit (IMU) readings, forming a Visual Inertial Odometry (VIO) system to achieve higher tracking accuracy, with IMU and VO complementing each other. Depending on the application, VIO can be extended to Visual Inertial Simultaneous Localization and Mapping (SLAM), enabling the detection of previously visited places as well as the optimization and retroactive correction of the predicted trajectory through place recognition [6], [8].

While both VIO and Visual Inertial SLAM algorithms have been deployed in a multitude of applications in robotics, automotive, and mixed reality, the current state-of-the-art algorithms are computationally expensive [9]. They typically require powerful computing platforms with power requirements ranging from watts to tens of watts [7], to process camera streams with 20 FPS to 50 FPS [10]. Since those computing platforms and the corresponding battery packs to power them can weigh hundreds of grams to kilograms, the application of state-of-the-art VIO in micro- and nano-drones, as well as in augmented reality glasses, is limited or prevented up to now [9], due to strict payload limitations.

Although modern VIO algorithms are not available on small-scale devices due to the challenges of computing at low latency on ultra-low-power processors, previous works reduced the full VIO problem to simpler formulations capable

of operating with less compute power. Among the least power-demanding implementations is the fully integrated Application Specific Integrated Circuit (ASIC) Navion [11], consuming down to 2 mW at 20 frames per second. Another example of highly constrained algorithms is the reduction of VIO to planar localization only [12], [13]. Further increasing power budget and relaxing algorithmic constraints, research utilizing Field Programmable Gate Arrays (FPGAs) or even Raspberry Pis has been shown to run VIO pipelines by using specialized hardware for optical flow extraction on-camera [14], or FPGA-based hardware accelerators [15].

Following up on these previous works to reduce the energy footprint of VIO towards accurate, infrastructure-less, and low power movement tracking, this work bridges the gap between the simplified algorithms typically used on constrained devices and accurate state-of-the-art algorithms, by proposing a fully featured and lightweight six Degrees of Freedom (DoF) VIO pipeline optimized to run on ultra-low power compute platforms. Additionally, this new VIO pipeline, termed *Lightweight Embedded Visual Inertial Odometry (LEVIO)*, is fully implemented in C code to be deployable on Commercial Off-The-Shelf (COTS) hardware and open-sourced.

The main contributions of *LEVIO* are:

- 1) **Efficient VIO Pipeline:** Through design space exploration, we propose a six DoF VIO pipeline termed *LEVIO*, which is lightweight and accurate. The *LEVIO* pipeline consists of established VIO components and algorithms like Oriented FAST and Rotated BRIEF (ORB) features and Bundle Adjustment (BA), while focusing on a slim, computationally efficient design, able to process image streams at 20 FPS.
- 2) **Hardware-Software Codesign:** The proposed *LEVIO* pipeline is further tailored towards embedded microcontrollers and System on a Chips (SoCs), with strict memory limitations and limited computational power in mind. Therefore, we highlight the relevant design choices and optimization for parallelization and memory management, resulting in a highly parallelizable algorithm to leverage modern multicore platforms and operate with a low memory footprint (below 256 kB for VO without optimization and below 1 MB for the whole pipeline).
- 3) **On-Hardware Validation:** As proof of concept, the proposed pipeline is validated in the form of an implementation for an existing ultra-low power RISC-V SoC with parallel processing capabilities, and thoroughly benchmarked against open-source VIO datasets for comparison with other literature. For the validation, the commercially available GAP9 SoC by GreenWaves Technologies has been chosen as a suitable platform.
- 4) **Open-Source:** To support further advancements in lightweight VIO, we open-source the full implementation of *LEVIO* here: <https://github.com/ETH-PBL/levio>

This work is organized as follows: Section II presents and reviews related work on influential VIO pipelines and pipelines targeting resource-constrained systems. Section III details the *LEVIO* pipeline and the necessary embedded optimizations

to target a low-power SoC. Sections IV and V cover the evaluation setup and experimental results. Section VI discusses the implications and limitations of the presented approach. Section VII concludes this work.

## II. RELATED WORK

In this section, we present the previous work related to our VIO approach. Both VIO and Visual Inertial SLAM have been extensively studied; therefore, we limit the related work section to the most influential works as well as to the works on which we base our *LEVIO* pipeline. Since our work aims to bridge the GAP between accurate and powerful approaches, as well as approaches targeted at resource-constrained devices, we introduce the corresponding work in separate subsections.

### A. Influential Visual Inertial Odometry Works

Among the active research areas of VO, VIO, and Visual-Inertial SLAM (VI-SLAM), which are frameworks for estimating motion and building a map of the environment, a wide variety of algorithms have been proposed, each with different trade-offs and design philosophies. These systems can be classified along several key dimensions:

- **Direct vs. Indirect vs. Hybrid Tracking:** This refers to how visual information is processed. Indirect (or feature-based) methods extract and match visual features (e.g., corners, descriptors), whereas direct methods work directly on raw pixel intensities by minimizing the photometric error. Hybrid methods combine aspects of both.
- **Filtering vs. Optimization:** Filtering approaches (e.g., Extended Kalman Filter (EKF)) process data sequentially and recursively, while optimization-based approaches (e.g., BA) refine state estimates over a window of data or keyframes using non-linear optimization.
- **Loop Closure:** Indicates whether a system includes the ability to recognize and correct for revisiting previously seen locations to reduce long-term drift.
- **Coupling Strategy:** Describes how the camera and inertial measurements are fused. *Tightly coupled* systems jointly estimate motion using both modalities in a unified framework, while *loosely coupled* systems process them separately and fuse results at a higher level.
- **Sensor Setup:** Encompasses the use of monocular, stereo, or RGB-D cameras, which affects scale and depth observability, initialization, and robustness.

These dimensions greatly affect a system's accuracy, robustness, real-time capability, and suitability for resource-constrained platforms. We subsequently describe several influential works in the field of VIO and VI-SLAM, using these dimensions as a framework for comparison. One key similarity among these algorithms is their computational complexity, which typically requires desktop computers for real-time position estimation.

One of the earliest and most well-known indirect, filtering-based VIO systems is MSCKF [19], proposed in 2007. It adopts a tightly coupled design, using an EKF to fuse tracked visual SIFT [20] features with IMU measurements. MSCKF does not support loop closure and relies on a monocular

TABLE I

COMPARISON OF LOW-POWER VO AND VIO IMPLEMENTATIONS ACROSS EMBEDDED PLATFORMS. THE SYSTEMS ARE ORDERED BY INCREASING POWER REQUIREMENTS. THE DIVIDER LINE FURTHER SEPARATES SYSTEMS RUNNING EITHER ON BARE-METAL OR ON AN EMBEDDED OPERATING SYSTEM (OS) (ABOVE THE DIVIDER LINE) FROM THOSE SYSTEMS UTILIZING A FULLY FEATURED LINUX OS (BELOW THE DIVIDER LINE).

System / Work	Year	Type	Power ↓	Frame Rate ↑	Processor / Platform
Navion [11]	2019	Monocular VIO	2 mW	20 FPS	Custom ASIC
Parallelized PX4FLOW [13]	2022	2D Optical Flow	25 mW	500 FPS	GreenWaves GAP8 SoC
PX4FLOW [12]	2013	2D Optical Flow	<100 mW	250 FPS	ARM Cortex-M4F
PicoVO [16]	2021	Monocular VO	310 mW	33 FPS	ARM Cortex-M7
Bahnam <i>et al.</i> [17]	2021	Stereo VIO (MSCKF)	Not stated	Not stated	RPi Zero
Gu <i>et al.</i> [15]	2022	VO (Hybrid FPGA+CPU)	2.6 W	20 FPS	Zynq Ultrascale+ ZU3EG
Kühne <i>et al.</i> [14]	2024	VIO	3.8 W	50 FPS	RPi CM4 + On-Sensor Acceleration
BotVIO [18]	2025	Monocular VIO (Transformer-Based)	5.4 W	57.8 FPS	NVIDIA Jetson Xavier NX

camera setup. At the time of publication, it was capable of operating at 14 Hz on a single-core 2 GHz desktop processor, demonstrating real-time feasibility.

ROVIO [10] is a subsequent evolution within the same class of systems (indirect, filtering-based, tightly coupled), but it adopts a more computationally efficient approach. Instead of detecting and matching features, it tracks small image patches (i.e., pixel templates) directly within the EKF framework, thus resembling a hybrid method. ROVIO is designed for monocular cameras and omits loop closure. It can process around 50 tracked patches in approximately 30 ms per frame on a single core of an Intel i7-2760QM.

To improve long-term accuracy, several systems implement loop closure in addition to VIO. A prominent example is OKVIS (2015) [21], a tightly coupled, indirect, optimization-based VI-SLAM system. OKVIS uses a stereo or monocular camera setup, tracks Harris [22] corners, and describes them using BRISK descriptors [23]. The system employs a sliding-window approach for local BA and includes loop closure for global consistency. It achieves real-time performance on a quad-core Intel Core i7 at 2.2 GHz.

In contrast to the works presented above, VI-DSO [24] represents a shift toward direct, optimization-based methods. It tracks camera motion by minimizing the photometric error across frames without relying on keypoint extraction or descriptors. The system uses a tightly coupled fusion of inertial and visual data within a non-linear optimization framework. VI-DSO supports monocular input and does not perform loop closure. The absence of feature extraction improves runtime performance and robustness in low-texture environments.

VINS-Mono [25] is another indirect, optimization-based, tightly coupled VI-SLAM system. It employs KLT optical flow [26] to track features across frames and maintains a sliding window for non-linear optimization. VINS-Mono supports monocular cameras and includes a robust loop closure and relocalization mechanism via pose-graph optimization. It was demonstrated to run in real-time on an Intel Core i7-5500U.

Concluding the enumeration of influential VIO works, ORB-SLAM3 [27] is one of the most complete and flexible indirect, optimization-based VI-SLAM systems. It supports monocular, stereo, and RGB-D inputs, with optional integration of IMU data. ORB-SLAM3 performs full BA and includes

robust loop closure, relocalization, and map reuse. It uses ORB features [28] for tracking and mapping, which provide a good trade-off between speed and robustness. Thanks to its modularity and performance, it achieves real-time operation on an Intel Core i7-7700 (3.6 GHz) and has become a widely used baseline in the community.

A comprehensive overview and comparison of these and other state-of-the-art systems is provided by Macario *et al.* [6], including a taxonomy and benchmarking results across datasets and hardware platforms.

To achieve an accurate six DoF VIO pipeline, we draw inspiration from current state-of-the-art VIO pipelines like VINS-Fusion [25] and ORB-SLAM3 [27], and extract the technological advances that led to the most significant performance improvements. Given the strict hardware limitations in compute and memory on an ultra-low-power SoC like the targeted GAP9 SoC, we aim to implement the algorithms and pipeline segments that yield high accuracy improvements at moderate computational requirements, while leaving out expensive computations that are used in the top-performing VIO pipelines.

### B. VIO for Resource-Constrained Devices

Among resource-constrained devices, we review the broad range of VIO implementations from microcontrollers in the mW-range up to single-board computers in the single-digit W-range and summarize the key findings in Table I. VIO implementations for microcontrollers typically utilize simplified approaches to achieve low energy consumption. One prime example is PX4FLOW [12]. The algorithm is restricted to 2D planar motion and calculates Optical Flow (OF) by matching image patches between frames. This reduces computational effort with respect to more complex feature detectors like ORB [29], but limits the speed at which features can move between two consecutive camera frames. Due to these optimizations, PX4FLOW achieves up to 250 Hz update rates while running on a Cortex M4F processor. An extension of this principle is presented by [13] on a state-of-the-art SoC GAP8, improving the PX4FLOW algorithm to run at up to 500 Hz, while consuming only 25 mW.

Increasing complexity to 3D tracking, PicoVO [16] presents the feasibility of running VO-only on an ARM Cortex M7 with

up to 33 FPS at 310 mW.

The system called Navion [11] further enhances the algorithmic capabilities to a full six DoF VIO system. This work consumes an average of 2 mW while processing 20 FPS thanks to its fully custom-designed ASIC chip.

Similarly to the custom ASIC implementation, when allowing more capable algorithms and compute platforms, one option to still reduce power consumption is to offload computationally expensive tasks to dedicated hardware. In this domain [15] presents an FPGA SoC approach based on an AMD Zynq UltraScale+ ZU3EG, where the compute-intensive Harris corner detection is implemented on the programmable logic part, while the rest of the pipeline resides in the programmable system part of the chip. Overall, the system power consumption is 2.6 W with a processing time for the frontend of 28.7 ms, allowing 20 FPS. A similar idea of offloading computation is presented in [14], which integrates a camera with on-sensor processing capabilities. The camera pre-processes images and outputs the calculated optical flow, which is being used by the VINS-Mono [25] pipeline to estimate VIO. The overall system can process up to 50 FPS on a Raspberry Pi Compute Module 4, consuming 3.8 W. Similarly, an extended algorithm also containing stereo matching (MSCKF) was optimized for an RPi Zero compute module in [17].

Notably, the presented approaches all rely on classical image processing. While machine learning approaches exist, the most recent and optimized designs, like BotVIO [18], still require a significant amount of power and memory to achieve competitive accuracy. While BotVIO is able to run on a NVIDIA Jetson NX, where only two of the six CPU cores are utilized, it relies on the integrated GPU cores to achieve its top framerate of 57.8 FPS at 5.4 W.

This work advances the state of the art, proposing an efficient six DoF VIO pipeline that can be deployed on a low-power SoC using less than 100 mW, while reaching 20 FPS.

### III. METHODOLOGY

The *LEVIO* system architecture is guided by a constraint-driven design approach, where the inherent limitations of the targeted ultra-low-power GAP9 SoC, such as its constrained memory and multicore cluster architecture, led to key innovations within the VIO pipeline. Unlike VIO systems designed for desktop platforms, which prioritize accuracy and feature density, *LEVIO*'s design choices were made to ensure real-time performance at sub-100 mW power consumption. In the following subsections, we integrate the description of the VIO pipeline with a detailed explanation of how these hardware constraints directly shaped our methodology and optimization strategies.

To efficiently explore the design space, we implemented a golden model of *LEVIO* in Python. This model was used to validate and benchmark the *LEVIO* pipeline in terms of accuracy improvements and robustness towards changing parameter configurations. This allows us to design and optimize the *LEVIO* system, validating the performance gain of possible pipeline segments before incorporating them into the final

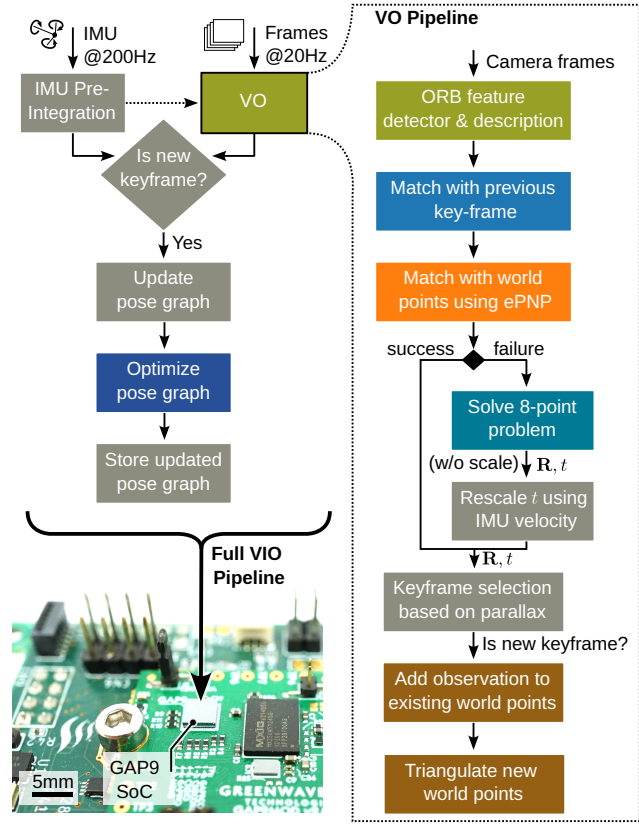


Fig. 1. Blockdiagram of the *LEVIO* pipeline. The overview of the full VIO pipeline is depicted on the left, with a detailed description of the VO segments to the right. The complete pipeline has been verified using a Python golden model and is deployed on the GAP9 SoC.

design. The Python golden model is used for algorithmic design-space exploration and parameter sweeps.

Once we obtained the final pipeline architecture (section III-A), we further tailored it towards ultra-low-power multicore SoCs and microcontrollers. The modifications required to deploy the pipeline on a SoC with less than 1 MB of memory, as well as the optimization necessary to run the pipeline at typical VIO real-time frame-rates of 20 FPS are described in section III-D. We verify the applicability to real-world embedded systems by implementing and benchmarking the *LEVIO* pipeline on a commercially available SoC. The embedded system runs a self-contained C implementation based on the best-performing Python golden model.

#### A. The Proposed VIO Pipeline

Following the terminology introduced in section II-A, the *LEVIO* pipeline, depicted in Figure 1, utilizes feature-based (indirect) motion estimation using ORB features [28]. To estimate relative movements from frame to frame, the 8-point algorithm is used, whereas for estimating the camera pose relative to 3D landmarks, the Efficient Perspective-n-Point (EPnP) algorithm [30] is employed. *LEVIO* uses a pose-graph optimization approach to refine the odometry estimates. To obtain a pose-graph that can be efficiently and accurately optimized, a keyframe selection scheme is employed. To select frames with a sufficiently large baseline for accurate landmark

triangulation and pose-graph optimization, keyframes are only introduced once a certain parallax threshold between the current frame and the previous keyframe is exceeded. The pose-graph optimization is formulated as a tightly coupled problem, where BA of VO estimates and the fusion of pre-integrated IMU measurements are jointly executed to obtain a VIO estimate. Due to the limited memory on the SoC platform, loop closure is omitted, and a monocular camera setup is used.

The characteristics of each pipeline segment, as well as our design decisions, are detailed in the subsequent section III-B and section III-C.

### B. VO Pipeline Segments

The VO pipeline depicted on the right side of Figure 1 is composed of the following segments:

- 1) **ORB:** For feature detection and description, we selected ORB [28], as it offers a good trade-off between computational efficiency and relevant descriptor properties like re-detectability and uniqueness. The layered approach of efficiently computing the FAST score [31] on each pixel, while only computing the Harris score [22] on FAST corners, allows for efficient computation and is well-suited for parallelization. The same is true for the computation of ORB descriptors, which are only computed on valid Harris corners.
- 2) **Feature Matching:** Feature matching between two frames, as well as between frames and world points, is performed using a two-way brute-force matcher. Given the relatively small number of descriptors (up to 700 for frames and up to 1000 for the world points), this can be done efficiently and is also well parallelizable.
- 3) **8-point RANdom SAmple Consensus (RANSAC):** The relative motion between two frames is estimated using the 8-point essential matrix computation [32]. The essential matrix,  $E$ , links normalized point correspondences  $(x_i, x'_i)$  through the epipolar constraint:

$$x_i^\top E x'_i = 0 \quad (1)$$

$E$  is estimated using least-squares, and its rank is constrained to 2. The final rotation ( $R$ ) and translation ( $t$ ) are extracted from the essential matrix within a RANSAC loop [33] to obtain an accurate solution in the presence of outliers. The use of RANSAC allows for straightforward parallelization of the essential matrix estimation by distributing RANSAC iterations to different cores. The motion estimation between two frames is performed to bootstrap the VIO pipeline, i.e., to initialize the pipeline or when not enough feature matches between the current frame and the world points are found.

- 4) **EPnP RANSAC:** To determine the perspective of the current frame relative to 3D landmarks, matches between image points and world points (landmarks) are needed. The camera's absolute pose ( $R, t$ ) is determined by mapping 3D world landmarks ( $X_j$ ) to their 2D image projections ( $x_j$ ) using the efficient EPnP algorithm [30]. EPnP solves the 2D-3D correspondence problem by expressing 3D points as a linear combination of four

virtual control points. In this case, RANSAC is also used to find an accurate solution in the presence of outliers. Single RANSAC iterations can be distributed to different cores to achieve parallel execution. In the case where not enough matches between world points and the current frame are found (default threshold value of 25), EPnP RANSAC is not executed, and the motion estimation falls back to 8-point RANSAC.

- 5) **Simple Keyframe Selection:** To reduce the number of frames that are being tracked in the pose-graph, while still keeping enough data for spatio-temporally consistent BA, we employ a simple keyframe selection scheme. A frame is selected to be a keyframe and added to the pose-graph once a certain parallax threshold between the current frame and the previous keyframe is exceeded.
- 6) **Triangulation and Tracking of World Points:** Once a new keyframe is added, the correspondences (observations) between the new keyframe and the world points are registered. Furthermore, the feature matches between the current and the previous keyframe are used to triangulate previously unobserved world points.

### C. IMU and Optimization Pipeline Segments

The remaining VIO segments depicted on the left side of Figure 1 are required for the processing of IMU readings and the pose-graph optimization, which simultaneously performs BA and jointly optimizes the IMU constraints and the VO constraints. The pipeline segments are the following:

- 1) **Maintaining the Pose-Graph:** To be able to perform BA, which optimizes the pose-graph, we must maintain a pose-graph consisting of poses and world points [6]. The observations form the edges between these poses and world points. Furthermore, to account for the IMU data, each pose contains additional velocity and IMU-bias states, and the pre-integrated IMU measurements form the edges between two consecutive poses and their respective states.
- 2) **IMU Pre-Integration:** To account for both effects of IMU measurements arriving at different rates than image frames and keyframes being selected at irregular intervals, we employ IMU pre-integration [34] to obtain only one IMU constraint between two keyframes. Measurements between keyframes  $k$  and  $k+1$  are pre-integrated into single relative motion constraints. Let  $R$ ,  $p$ , and  $v$  be the rotation, position, and velocity of the body frame, respectively, and  $\Delta t$  be the total time interval.  $g$  is the gravity vector, and  $\Delta \hat{R}$ ,  $\Delta \hat{v}$ , and  $\Delta \hat{p}$  are the pre-integrated measurements for rotation, velocity, and position. This process yields the following residuals, which are minimized during optimization:

$$r_R = \log((\Delta \hat{R})^\top R_k^\top R_{k+1}) \quad (2)$$

$$r_v = R_k^\top (v_{k+1} - v_k - g\Delta t) - \Delta \hat{v} \quad (3)$$

$$r_p = R_k^\top (p_{k+1} - p_k - v_k \Delta t - \frac{1}{2} g \Delta t^2) - \Delta \hat{p} \quad (4)$$

- 3) **Pose-Graph Optimization** The BA of the VO estimates and the fusion with the pre-integrated IMU data is

formulated as a tightly coupled optimization problem. Whenever a new keyframe is added, we stop the current IMU pre-integration and add both the new observation and IMU constraints to the optimization problem. The optimization problem is formulated as a moving window on the pose-graph, only optimizing the most recent keyframes. The oldest keyframe states (pose, velocity, and bias) serve as initial conditions and are further anchored by additional constraints.

#### D. Deployment Optimizations

Moving from the Python-based golden model to ultra-low-power embedded platforms, the following functional additions and changes were necessary to run *LEVI*O. To verify the applicability of *LEVI*O to ultra-low-power embedded systems, we target the specifications of the commercially available GAP9 SoC. GAP9 hosts a nine-core compute cluster comprising a master core and eight worker cores, as well as an additional fabric controller core responsible for interacting with peripherals and external memories. Operating at its maximum frequency of 370 MHz GAP9 uses less than 100 mW [35], [36].

**1) Custom Linear Algebra Library:** To our knowledge, there is no linear algebra library available in C that supports advanced operations like Singular Value Decomposition (SVD) or the Jacobi Eigenvalue algorithm, which is compact enough to be deployed on an SoC like GAP9. Established feature-rich libraries like LAPACK [37] could not be run on GAP9. Therefore, we built a custom linear algebra library that supports SVD of square matrices, the Jacobi Eigenvalue algorithm, the Inverse Power method, and a selection of solvers for systems of linear equations.

**2) Hierarchical Memory Handler:** The memory hierarchy of GAP9 consists of 128 kB of L1 memory, which is accessible by the compute cluster and 1.6 MB of L2 memory only accessible by the fabric controller. While the 128 kB is sufficient to store the required values for the function or pipeline segment being executed at any given time, it is not enough to store all relevant data, most notably the pose-graph and the data of the previous keyframe. Therefore, we allocate designated space for this data in the L2 memory and move it into the L1 memory when needed. The L1 memory is mainly used as a scratchpad, and no data is preserved between iterations.

**3) Reduced Image Resolution:** Given the 128 kB limitation of the L1 memory, we decided to use QQVGA (160 pixels by 120 pixels) resolution for the image inputs, to have sufficient work memory available for the online computations.

**4) Adapted Optimizer Formulation:** The VIO problem is formulated as a Maximum a Posteriori (MAP) estimation solved with the Levenberg–Marquardt (LM) algorithm. To make the optimization problem tractable on a SoC, we exploit the problem’s sparse structure using the Schur complement [38] on the full system of normal equations. The full Hessian matrix  $H$  and the corresponding right-hand side vector  $b$  are partitioned based on the two types

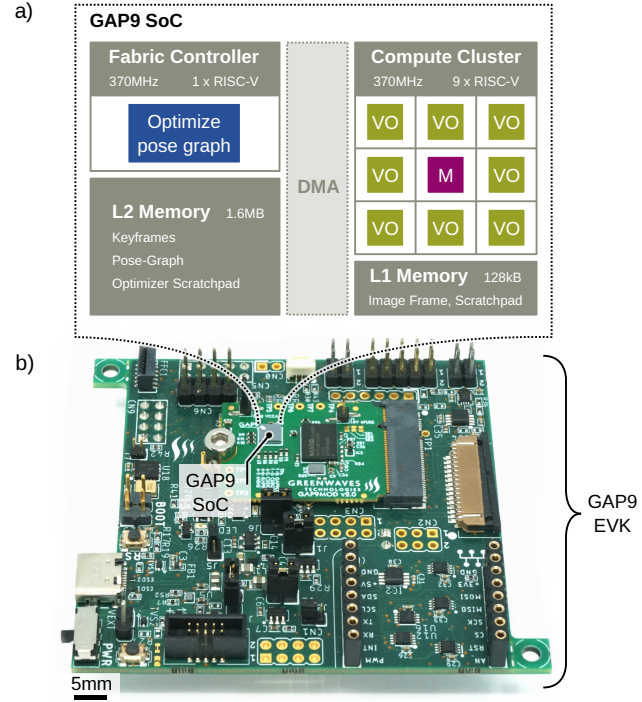


Fig. 2. a) Block diagram presenting the hardware resources of the GAP9 SoC and tasks of the *LEVI*O pipeline, with the pose graph optimization running on the fabric controller and the VO mapped to the eight parallel processing cores. Non-parallelized parts of the VO are handled by the Master Core (M). b) Overview of the physical GAP9 Evaluation Kit (EVK).

of states: the camera pose states ( $p_p$ ) and the 3D landmark states ( $p_l$ ), with  $\delta p$  being the perturbation vector:

$$\begin{bmatrix} H_{pp} & H_{pl} \\ H_{lp} & H_{ll} \end{bmatrix} \begin{bmatrix} \delta p_p \\ \delta p_l \end{bmatrix} = \begin{bmatrix} b_p \\ b_l \end{bmatrix} \quad (5)$$

This marginalizes the 3D landmark states ( $p_l$ ), resulting in a much smaller, reduced system that solves only for the camera pose states ( $p_p$ ):

$$(H_{pp} - H_{pl}H_{ll}^{-1}H_{lp})\delta p_p = b_p - H_{pl}H_{ll}^{-1}b_l \quad (6)$$

Solving this condensed system drastically reduces computational and memory overhead. Furthermore, due to the high timing requirements for LM optimization, we do not sequentially execute the optimizer after a new keyframe has been added, but we continuously run the optimization on the fabric controller, largely independent of the VO iterations. However, the optimization problem is updated whenever a new keyframe is added.

**5) Parallelization:** We adapted most VO pipeline segments to be executable in a parallelized fashion. The ORB feature detection and description, as well as the brute-force matching logic, have been parallelized by processing subsets of the input data on different cores. Furthermore, both the 8-point and the EPnP RANSAC loops have been parallelized by processing single RANSAC iterations on different cores.

#### IV. EVALUATION

The evaluation of the *LEVIO* pipeline was performed both at an algorithmic level utilizing the Python golden model, and by analyzing its viability and employability on real-world embedded platforms by deploying the optimized C implementation on the GAP9 evaluation kit, as shown in Figure 2.

##### A. Performance Evaluation of the *LEVIO* Algorithm

To assess the algorithmic capabilities of the *LEVIO* system, we rely on the golden model as mentioned in section III-A, developed to estimate how the addition or removal of certain pipeline segments affects the overall prediction accuracy while also considering the computational requirements.

Therefore, we benchmark multiple pipeline configurations using the *EuRoC* dataset [39]. Furthermore, we performed an extensive parameter sweep on relevant VIO parameters to further increase the statistical relevance of the design space exploration. For each of the pipeline variants and parameter choices, the resulting trajectory estimate was evaluated using the *rpg\_trajectory\_evaluation*<sup>1</sup> tool [40]. We focus our analysis on the absolute Root Mean Square Error (RMSE), i.e., the RMSE over all predicted poses, as well as the relative translation error for multiple trajectory segments of 40 m, covering the full length of each trajectory. To obtain a single metric, we state the average error across all sampled segments.

##### B. Real World Embedded Evaluation of *LEVIO*

To verify that the *LEVIO* pipeline is viable for use on real-world resource-constrained systems, we deploy it on the GAP9 parallel ultra-low-power SoC by GreenWaves Technologies. While the deployed pipeline is conceptually the same as the golden model, some modifications and additions, as stated in section III-D, were necessary.

For the deployed pipeline on GAP9, we analyse the computational requirements in terms of cycle counts when executing *LEVIO* on a single core and when parallelizing the execution on the available eight worker cores. Additionally, we assess the achieved parallelization speedup for each of the parallelized code segments, as well as the overall performance.

Furthermore, we analyze the utilization of both the L1 and L2 memories. As we store the pose-graph persistently in L2 memory, this is a static number. On the contrary, for L1 and the L2 memory used as work memory by the pose-graph optimizer, we analyze the peak utilization for each pipeline segment.

##### C. Benchmark Dataset: *EuRoC*

For all system evaluations, we used the *EuRoC* dataset [39]. This dataset is a challenging standard in the VIO community, recorded on board a real drone under high-dynamic and variable-illumination conditions, making it the most application-relevant benchmark for the *LEVIO* system.

<sup>1</sup>[https://github.com/uzh-rpg/rpg\\_trajectory\\_evaluation](https://github.com/uzh-rpg/rpg_trajectory_evaluation)

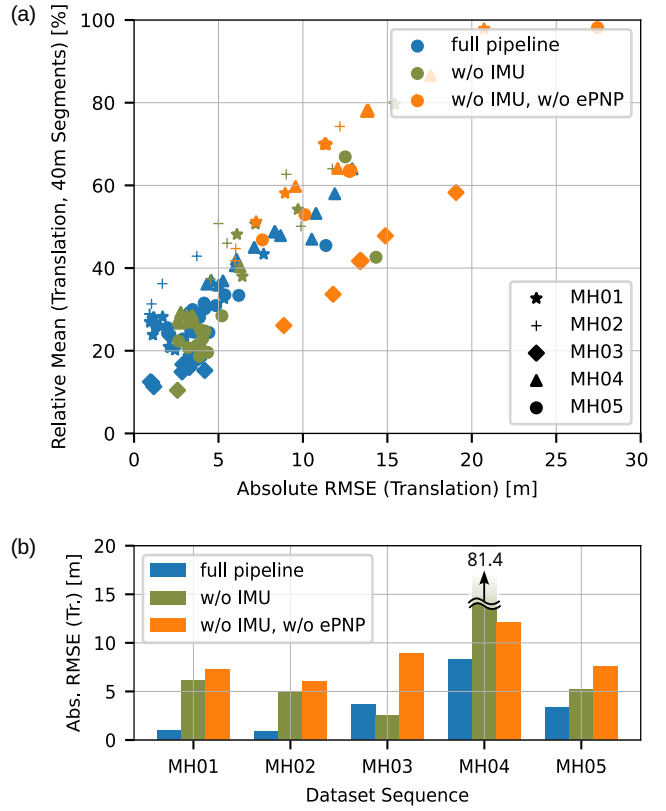


Fig. 3. Relative and absolute translation RMS error of the golden model during the parameter sweep (a) and absolute RMSE error for the best performing configuration, when applied to each sub-dataset (b). Data is color-coded for the type of pipeline, and the shapes indicate the dataset it was evaluated on (EuRoC MH01–MH05).

While *EuRoC* was recorded with a drone that is larger than the systems considered in this work, the used sensors are also representative of resource-constrained devices as considered in this work. *EuRoC* offers global-shutter stereo camera data at 20 Frames Per Second (FPS) and IMU readings at 200 Hz. Since those are typical data rates for VIO systems, we use them both in our golden model and the GAP9 deployment. We do, however, only use one camera, as *LEVIO* is a monocular VIO system. Additionally, we subsample the images when deploying the pipeline on GAP9.

## V. RESULTS

In this section, we present the results obtained from the algorithmic study performed using the golden model and the results and insights gained when deploying *LEVIO* on GAP9. For the algorithmic study, we performed an ablation study of varying VIO pipeline complexities to motivate the use of pipeline segments, as well as the parameter selection. For the deployment on GAP9, we report relevant metrics for both real-time robotic applications and resource usage, such as latency, memory usage, and parallelization performance.

##### A. Pipeline Evaluation

We analyzed three pipeline configurations as described below:

TABLE II

THE PERFORMANCE NUMBERS OF THE BEST PERFORMING PARAMETER SET FOR EACH PIPELINE CONFIGURATION IN TERMS OF RMSE, WHEN AVERAGING OVER THE FIVE *EuRoC* SEQUENCES. ADDITIONALLY, FOR THE FULL *LEVI*O PIPELINE, THE PERFORMANCE NUMBERS OF THE BEST-PERFORMING PARAMETER SET IN TERMS OF TRANSLATION ERROR ARE GIVEN. WHEREAS FOR THE OTHER TWO PIPELINE CONFIGURATIONS, THE BEST PERFORMING PARAMETER SETS IN TERMS OF RMSE AND RELATIVE TRANSLATION ERROR ARE IDENTICAL.

Pipeline Configuration	MH01		MH02		MH03		MH04		MH05	
	Abs. [m]	Rel. [%]								
<i>LEVI</i> O w/o IMU, w/o EPnP	7.228	51.23	5.982	41.77	8.867	26.10	12.061	64.10	7.601	46.80
<i>LEVI</i> O w/o IMU	6.092	48.14	4.995	50.77	<b>2.572</b>	<b>10.42</b>	81.374	282.09	5.202	28.45
Full <i>LEVI</i> O - Best Abs. Error	<b>0.963</b>	<b>26.96</b>	<b>0.920</b>	<b>28.86</b>	3.685	18.61	<b>8.334</b>	<b>48.77</b>	<b>3.376</b>	<b>28.29</b>
Full <i>LEVI</i> O - Best Rel. Error	1.115	23.83	4.431	19.36	2.843	14.89	10.781	57.98	3.467	29.96

- 1) **Full *LEVI*O Pipeline:** The full pipeline consists of all pipeline segments as described in section III and shown in Figure 1.
- 2) ***LEVI*O without IMU Data:** For the second configuration we reduced *LEVI*O to a VO-only configuration, where no IMU data is included in the optimization step.
- 3) ***LEVI*O without IMU Data and EPnP:** In this configuration, we reduce the system to the 8-point algorithm for frame-to-frame pose estimation and use keyframe selection and BA to optimize the result.

Furthermore, we used parameter sweeps across the following dimensions: 1) Optimization Window Size, 2) Keyframe Threshold, 3) Reprojection Error Noise Model, 4) IMU Noise Model, and 5) Gravity Vector Updates, where the last two parameters are only relevant for the full pipeline, where IMU data is being used.

The accuracy results of those benchmark sweeps are depicted in Figure 3. Furthermore, Figure 3b) indicates the best-performing parameter set for each pipeline configuration in terms of RMSE. In Table II, we list the performance figures of those three configurations in terms of RMSE. Additionally, we list the best-performing models in terms of relative translation error. For the full *LEVI*O pipeline, the best relative translation error is achieved by a different parameterization than the best RMSE.

One can observe that the most complex pipeline, Full *LEVI*O, reaches the highest accuracy when adequately parametrized, with an average RMSE of 3.46 m over all sequences. Additionally, Figure 3a) illustrates that the addition of IMU data mainly reduces long-term drift. This can be observed by the relative mean translation error of 40 m sub-trajectories being in a similar range for the full pipeline and the pipeline without IMU data, but the RMSE, which captures the full trajectory, being lower for the full pipeline. When looking at the data of the best performing configurations in Table II for MH05, we can observe that the relative error for both pipelines is nearly identical. In contrast, the absolute RMSE of the pipeline without IMU data is with 5.2 m versus 3.38 m approximately 54 % higher than for the full pipeline.

In Figure 3a), we can observe that depending on the parameterization, there is a trade-off between RMSE and relative translation error. The scatter plot indicates that the RMSE can be increased to, in turn, reduce the relative translation error. Depending on the application and whether short-term or long-term consistency is more important, this can be an interesting

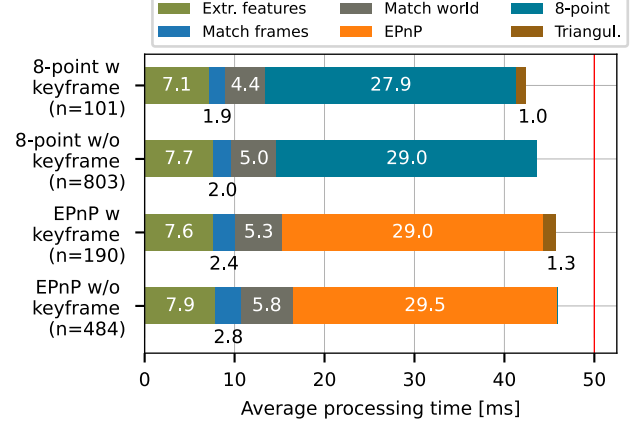


Fig. 4. Average runtime of the parallelized *LEVI*O pipeline for different scenarios occurring during processing (either EPnP or 8-point, and with/without keyframe). Small numbers showing the execution time in ms. On average, the pipeline processes incoming camera frames with a runtime below 50 ms, allowing for 20 FPS.

tuning parameter.

### B. Deployment on GAP9

To evaluate the real-time capabilities of *LEVI*O on GAP9, we analyzed the timing requirements for the VO part of the pipeline in Figure 4, with the computation limit imposed by a 20 FPS image stream indicated by the red line. To obtain statistical runtime data, we process the MH01 sequence on GAP9 (first 1578 frames). Using this real-world dataset yields a varying number of matches between the triangulated landmarks and the image frames or between two image frames. Given the varying number of matches, both the 8-point and the EPnP algorithm are executed regularly, in 57.3 % and 42.7 % of the VO iterations, respectively.

As can be seen from the timing analysis shown in Figure 4, the complexity of the full *LEVI*O pipeline over the configurations without IMU data and EPnP computation comes at a minimal latency overhead. To a great extent, this is due to the mutually exclusive execution of the EPnP and the 8-point algorithms. We only start EPnP when we have sufficiently many feature matches with landmarks; otherwise, the 8-point algorithm is executed. Both 8-point and EPnP RANSAC are computationally heavy, each utilizing between 62.9 % and 64.1 % of the computation time per iteration. Secondly, the overhead of the IMU pre-integration is minimal, contributing

TABLE III

BREAKDOWN OF AVERAGE COMPUTE CYCLES NEEDED WHEN PROCESSING THE *EuRoC* DATASET, IN CASE OF SINGLE CORE AND PARALLELIZED MULTICORE EXECUTION ON THE GAP9 PLATFORM

Pipeline Step	Single-Core [kCycles] ↓	Multi-Core [kCycles] ↓	Speed Up [Factor] ↑
Feature Extraction	21817	2926	7.46
Frame Matching	8112	1033	7.85
World Matching	16782	2128	7.89
EPnP RANSAC <sup>a</sup>	57324	10899	5.26
8-point RANSAC <sup>a</sup>	50391	10323	4.88
Triangulation <sup>b</sup>	374	374	1.00

<sup>a</sup>either EPnP or 8-point are calculated

<sup>b</sup>only done for keyframes, not parallelized

only 2.42 kCycles per IMU measurement, or 24.2 kCycles to pre-integrate the ten measurements obtained between two VO iterations, introducing an overhead of less than 0.15 %. Furthermore, the IMU pre-integration can be performed on either the cluster or the fabric controller.

The resulting parallelization speedup when running the VO pipeline on the eight worker cores of GAP9 versus the execution on a single core is shown in Table III. This comparison effectively isolates the algorithmic contributions from the hardware capabilities, demonstrating the performance advantages gained by fully utilizing *LEVIO*'s parallelization capability on the hardware platform. Furthermore, this architecture allows for highly efficient operating-point tuning: Since the processing throughput scales linearly with the clock frequency, the clock speed can be reduced linearly if a lower update rate (e.g., 10 FPS) is sufficient for the application. This capability enables the system to minimize dynamic power consumption while strictly adhering to the required real-time constraints.

For the feature extraction and both feature matching implementations (frame and world matching), the parallelization is very effective. In those cases, the parallelization is achieved by splitting the input data as evenly as possible across the eight worker cores. Additionally, the feature extraction and matching algorithms have a nearly constant runtime complexity. For both RANSAC algorithms, the parallelization is less effective. This is due to the fact that the parallelization is achieved by distributing the RANSAC iterations across the worker cores, while the runtime required for a single RANSAC iteration can vary significantly depending on the numerical conditioning of the randomly selected input samples. The runtime differences are caused by the underlying Jacobi Eigenvalue computation used for the SVD, which is an iterative algorithm whose convergence rate is strongly dependent on the input data. Thus, during each compute batch, the compute cluster needs to wait for all SVDs to converge before continuing. Furthermore, given the small computational cost, the triangulation of landmarks has not been parallelized.

The pose-graph optimization is computationally expensive at up to 55 MCycles or 15 ms per iteration, but can be performed independently of the VO estimation. Therefore, it is executed on the single fabric controller core, performing three

TABLE IV

MEMORY USAGE OF VARIOUS PIPELINE SEGMENTS OF *LEVIO*. L1 AND L2 INDICATE IN WHICH MEMORY SUBSYSTEM THE DATA IS STORED. FOR THE PIPELINE SEGMENTS THAT USE MORE WORK MEMORY, WHEN EXECUTED IN PARALLEL, WE INDICATE THE RESPECTIVE USAGE NEXT TO THE SINGLE-CORE USAGE.

Pipeline Step	Memory	Usage [kbyte] ↓ Single Parallel	Occupation [%] ↓ Single Parallel		
Feature Extraction	L1	64.0	50.03		
World Matching	L1	78.7	61.52		
EPnP RANSAC	L1	82.2	103.8	64.23	81.12
Frame Matching	L1	61.3	47.88		
8-point RANSAC	L1	65.6	69.2	51.26	54.08
Triangulation	L1	109.1	85.23		
Last Keyframe	L2	50.9	3.18		
Pose-Graph	L2	64.2	4.01		
Optimizer	L2	743.6	46.47		

optimizer iterations per VO iteration. Once a new keyframe is selected, the optimizer constraints are updated.

Regarding the memory utilization, we analyze the peak utilization for each pipeline segment in Table IV. Since we use the L1 memory as a scratchpad and only preserve the minimally necessary data between the pipeline segments, one can observe fluctuating memory occupation, but also a trend that an increasing amount of L1 memory is being used throughout a single VO iteration. At the end of the VO iteration, all data is transferred into the persistent L2 blocks storing the most recent keyframe and the pose-graph consisting of the eight most recent keyframe poses, the thousand most recent landmarks, and the corresponding observations linking the keyframe poses to the landmarks. To construct the full optimization problem, consisting of the Jacobian terms of each observation, the optimizer requires up to 743.6 kB of L2 memory.

## VI. DISCUSSION

This work demonstrates that full six DoF VIO can be achieved in real time on highly constrained embedded systems with memories in the MB-range and compute power in the range of giga-operations per second. *LEVIO* leverages visual tracking (ORB, EPnP) and inertial fusion techniques (IMU pre-integration, pose-graph optimization), while introducing a hardware-aware VIO pipeline optimized for parallel execution and low memory usage.

On the GAP9 SoC, *LEVIO* enables real-time performance at 20 FPS, benefiting from parallelized RANSAC loops, efficient memory management, and a lightweight custom optimizer for BA. While framerates of 20 Hz are typical and sufficient for most VIO tasks [39], the *LEVIO* pipeline is suitable for higher framerates, when deployed on corresponding hardware.

In terms of efficiency, highly power-efficient VIO pipelines can be realized using specialized ASICs (e.g. Navion [11]). However, the development is expensive and offers little to no reconfigurability to adapt to algorithmic advances. Being implemented on a general-purpose multicore SoC, the presented *LEVIO* implementation strikes a strong balance between software specialization and reconfigurability. Thus,

**TABLE V**  
ABSOLUTE TRAJECTORY ERROR (ATE) RMSE [M] ON EURoC MAV SEQUENCES (MACHINE HALL).

Method	Res.	LC	Sequence (ATE RMSE [m])				
			MH_01	MH_02	MH_03	MH_04	MH_05
LEVIO	Std.	No	0.96	0.92	3.69	8.33	3.38
LEVIO	QVGA	No	1.82	1.44	2.10	7.49	4.48
ORB-SLAM3	Std.	Yes	0.15	0.18	0.27	0.37	0.27
ORB-SLAM3	QVGA	Yes	0.18	0.22	0.26	1528.13	0.93
VINS-Mono	Std.	No	0.20	0.23	0.32	0.47	0.41
VINS-Mono	QVGA	No	0.25	0.18	0.46	0.47	0.60
VINS-Mono	Std.	Yes	0.14	0.16	0.30	0.34	0.34
VINS-Mono	QVGA	Yes	0.25	0.18	0.40	0.41	0.54

*LEVIO* stands out for providing highly efficient full six-DoF VIO estimation without requiring ASICs, Graphics Processing Units (GPUs), or simplified motion models.

Furthermore, the results demonstrate that classical single-core microcontrollers are currently incapable of executing a fully featured VIO pipeline in real-time (requiring roughly 300 ms per iteration at 370 MHz). *LEVIO* highlights the growing potential of lightweight multicore platforms to serve as a practical and scalable foundation for robotics and autonomous systems operating under tight resource constraints.

#### A. Comparison with Influential VIO Systems

We benchmark *LEVIO* against VINS-Mono [25] and ORB-SLAM3 [27] on the EuRoC dataset (see table V), evaluating the baselines at both standard (WVGA) and downscaled (QVGA) resolutions. A fundamental distinction lies in the algorithmic scope: while the baselines rely on Loop Closure (LC) to correct global drift, achieving sub-meter accuracy (< 0.3 m), *LEVIO* functions as a pure VIO pipeline, prioritizing constant-time processing over global consistency. The results expose the fragility of desktop-class algorithms under embedded constraints, with ORB-SLAM3 failing catastrophically on MH\_04 at QVGA resolution. Conversely, *LEVIO* trades absolute accuracy (yielding 0.9–3.5 m error) for strict robustness within a 100 mW power envelope. This represents a projected 15× efficiency gain over VINS-Mono running on systems like the Jetson Nano, confirming *LEVIO* as a viable solution for micro-drone stabilization where low-latency availability outweighs the need for global mapping.

#### B. Comparison with Ultra-Low-Power VIO

The landscape of ultra-low-power VIO and VO systems presents a trade-off between power consumption, computational complexity, and full 6 DoF capability, as shown in Table I. *LEVIO* occupies a unique niche by offering a full 6 DoF VIO pipeline with advanced features within the sub-100 mW range on COTS hardware. A comparison with low-power approaches highlights this differentiation:

- *Navion* [11] achieves ultra-low power (2 mW) utilizing a custom ASIC, which is less accessible and flexible than *LEVIO*'s COTS platform.

- *PX4FLOW & Parallelized PX4FLOW* [12], [13] operate at <100 mW but are limited to simplified 2D planar motion using basic optical flow, unlike *LEVIO*'s full 6 DoF capability.

- *PicoVO* [16] is a 3D Monocular VO system requiring higher power (310 mW). *LEVIO* runs at a significantly lower power point and includes inertial fusion (VIO), which enhances accuracy compared to VO-only methods.

In essence, *LEVIO* resolves the trade-off by delivering high algorithmic complexity on an accessible, ultra-low-power COTS platform, avoiding the compromises of custom hardware, power requirements, or algorithmic simplification common in similar embedded systems.

## VII. CONCLUSION

We presented *LEVIO*, a lightweight and fully embedded VIO pipeline optimized for ultra-low-power platforms with power envelopes below 100 mW. *LEVIO* achieves robust six DoF tracking while operating within tight computational and memory budgets (using less than 110 kB L1 and  $\approx$ 850 kB L2 memory), offering a compelling balance between efficiency and accuracy. While it does not aim to compete with high-end VIO systems, *LEVIO* demonstrates that practical, infrastructure-free localization is achievable on resource-constrained devices. This work further demonstrates that parallelization is a valid approach to enable real-time VIO at 20 FPS, suitable for nano drones and smart glasses. Validated on the public *EuRoC* dataset and deployed on GAP9, it enables real-time performance on microcontroller and ultra-low-power SoC hardware. Additionally, it is available as open-source for further research.

While *LEVIO* achieves impressive efficiency by successfully implementing a full VIO pipeline on an ultra-low-power SoC, the current system has several limitations that guide future research. To meet the strict power and memory budgets, *LEVIO* currently relies on very low-resolution (QQVGA) images and forgoes loop closure, which may limit long-term global consistency in large-scale environments. Future research will investigate the following open challenges: 1) loop-closure under tight memory constraints, 2) resolution–accuracy scaling beyond QVGA inputs, and 3) the design of hardware accelerators for typical VIO operations, such as SVD, feature extraction, or sparse matrix solvers. Additionally, we aim to extend *LEVIO*'s validation to more diverse real-world scenarios and to investigate portability to other low-power embedded architectures.

## REFERENCES

- [1] L. Rana and J. G. Park, “An enhanced indoor positioning method based on rtt and rss measurements under los/nlos environment,” *IEEE Sensors Journal*, 2024.
- [2] A. Sesyuk, S. Ioannou, and M. Raspopoulos, “A survey of 3d indoor localization systems and technologies,” *Sensors*, vol. 22, no. 23, p. 9380, 2022.
- [3] J. Sun, W. Sun, X. Zhang, J. Zheng, C. Tang, and Z. Chen, “Multiuser smartphone-based localization by composite fingerprint descriptors in large indoor environments,” *IEEE Sensors Journal*, vol. 23, no. 18, pp. 21 882–21 893, 2023.

[4] T. Laadung, S. Ulp, M. M. Alam, and Y. Le Moullec, "Novel active-passive two-way ranging protocols for uwb positioning systems," *IEEE Sensors Journal*, vol. 22, no. 6, pp. 5223–5237, 2021.

[5] T. Savić, X. Vilajosana, and T. Watteyne, "Constrained localization: A survey," *IEEE Access*, vol. 10, pp. 49 297–49 321, 2022.

[6] A. Macario Barros, M. Michel, Y. Moline, G. Corre, and F. Carrel, "A comprehensive survey of visual slam algorithms," *Robotics*, vol. 11, no. 1, p. 24, 2022.

[7] B. Xu, X. Li, J. Wang, C. Yuen, and J. Li, "Pvi-dso: Leveraging planar regularities for direct sparse visual-inertial odometry," *IEEE Sensors Journal*, vol. 23, no. 15, pp. 17 415–17 425, 2023.

[8] A. Merzlyakov and S. Macenski, "A comparison of modern general-purpose visual slam approaches," in *2021 IEEE/RSJ International Conference on Intelligent Robots and Systems (IROS)*. IEEE, 2021, pp. 9190–9197.

[9] Q. Zeng, H. Yu, X. Ji, X. Tao, and Y. Hu, "Fast and robust semidirect monocular visual-inertial odometry for uav," *IEEE Sensors Journal*, vol. 23, no. 20, pp. 25 254–25 262, 2023.

[10] M. Bloesch, S. Omari, M. Hutter, and R. Siegwart, "Robust visual inertial odometry using a direct ekf-based approach," in *2015 IEEE/RSJ international conference on intelligent robots and systems (IROS)*. IEEE, 2015, pp. 298–304.

[11] A. Suleiman, Z. Zhang, L. Carlone, S. Karaman, and V. Sze, "Navion: A 2-mw fully integrated real-time visual-inertial odometry accelerator for autonomous navigation of nano drones," *IEEE Journal of Solid-State Circuits*, vol. 54, no. 4, pp. 1106–1119, 2019.

[12] D. Honegger, L. Meier, P. Tanskanen, and M. Pollefeys, "An open source and open hardware embedded metric optical flow cmos camera for indoor and outdoor applications," in *2013 IEEE International Conference on Robotics and Automation*. IEEE, 2013, pp. 1736–1741.

[13] J. Kühne, M. Magno, and L. Benini, "Parallelizing optical flow estimation on an ultra-low power risc-v cluster for nano-uav navigation," in *2022 IEEE International Symposium on Circuits and Systems (ISCAS)*. IEEE, 2022, pp. 301–305.

[14] J. Kühne, M. Magno, and L. Benini, "Low latency visual inertial odometry with on-sensor accelerated optical flow for resource-constrained uavs," *IEEE Sensors Journal*, vol. 25, no. 5, pp. 7838–7847, 2025.

[15] P. Gu, Z. Meng, and P. Zhou, "Real-time visual inertial odometry with a resource-efficient harris corner detection accelerator on fpga platform," in *2022 IEEE/RSJ International Conference on Intelligent Robots and Systems (IROS)*. IEEE, 2022, pp. 10 542–10 548.

[16] Y. He, Y. Wang, C. Liu, and L. Zhang, "Picovo: A lightweight rgb-d visual odometry targeting resource-constrained iot devices," in *2021 IEEE International Conference on Robotics and Automation (ICRA)*. IEEE, 2021, pp. 5567–5573.

[17] S. Bahnam, S. Pfeiffer, and G. C. de Croon, "Stereo visual inertial odometry for robots with limited computational resources," in *2021 IEEE/RSJ International Conference on Intelligent Robots and Systems (IROS)*. IEEE, 2021, pp. 9154–9159.

[18] W. Wei, Y. Zhou, Y. Hu, Z. Li, S. Wang, X. Liu, and J. Li, "Botvio: A lightweight transformer-based visual-inertial odometry for robotics," *IEEE Transactions on Robotics*, 2025.

[19] A. I. Mourikis and S. I. Roumeliotis, "A multi-state constraint kalman filter for vision-aided inertial navigation," in *Proceedings 2007 IEEE international conference on robotics and automation*. IEEE, 2007, pp. 3565–3572.

[20] D. G. Lowe, "Object recognition from local scale-invariant features," in *Proceedings of the seventh IEEE international conference on computer vision*, vol. 2. Ieee, 1999, pp. 1150–1157.

[21] S. Leutenegger, S. Lynen, M. Bosse, R. Siegwart, and P. Furgale, "Keyframe-based visual-inertial odometry using nonlinear optimization," *The International Journal of Robotics Research*, vol. 34, no. 3, pp. 314–334, 2015.

[22] C. Harris, M. Stephens *et al.*, "A combined corner and edge detector," in *Alvey vision conference*, vol. 15, no. 50. Citeseer, 1988, pp. 10–5244.

[23] S. Leutenegger, M. Chli, and R. Y. Siegwart, "Brisk: Binary robust invariant scalable keypoints," in *2011 International conference on computer vision*. Ieee, 2011, pp. 2548–2555.

[24] L. Von Stumberg, V. Usenko, and D. Cremers, "Direct sparse visual-inertial odometry using dynamic marginalization," in *2018 IEEE International Conference on Robotics and Automation (ICRA)*. IEEE, 2018, pp. 2510–2517.

[25] T. Qin, P. Li, and S. Shen, "Vins-mono: A robust and versatile monocular visual-inertial state estimator," *IEEE transactions on robotics*, vol. 34, no. 4, pp. 1004–1020, 2018.

[26] B. D. Lucas and T. Kanade, "An iterative image registration technique with an application to stereo vision," in *IJCAI'81: 7th international joint conference on Artificial intelligence*, vol. 2, 1981, pp. 674–679.

[27] C. Campos, R. Elvira, J. J. G. Rodríguez, J. M. Montiel, and J. D. Tardós, "Orb-slam3: An accurate open-source library for visual, visual-inertial, and multimap slam," *IEEE transactions on robotics*, vol. 37, no. 6, pp. 1874–1890, 2021.

[28] E. Rublee, V. Rabaud, K. Konolige, and G. Bradski, "Orb: An efficient alternative to sift or surf," in *2011 International conference on computer vision*. Ieee, 2011, pp. 2564–2571.

[29] R. Mur-Artal and J. D. Tardós, "Orb-slam2: An open-source slam system for monocular, stereo, and rgb-d cameras," *IEEE transactions on robotics*, vol. 33, no. 5, pp. 1255–1262, 2017.

[30] V. Lepetit, F. Moreno-Noguer, and P. Fua, "Ep n p: An accurate o (n) solution to the p n p problem," *International journal of computer vision*, vol. 81, pp. 155–166, 2009.

[31] E. Rosten and T. Drummond, "Machine learning for high-speed corner detection," in *Computer Vision–ECCV 2006: 9th European Conference on Computer Vision, Graz, Austria, May 7–13, 2006. Proceedings, Part I 9*. Springer, 2006, pp. 430–443.

[32] H. C. Longuet-Higgins, "A computer algorithm for reconstructing a scene from two projections," *Nature*, vol. 293, no. 5828, pp. 133–135, 1981.

[33] M. A. Fischler and R. C. Bolles, "Random sample consensus: a paradigm for model fitting with applications to image analysis and automated cartography," *Communications of the ACM*, vol. 24, no. 6, pp. 381–395, 1981.

[34] C. Forster, L. Carlone, F. Dellaert, and D. Scaramuzza, "On-manifold preintegration for real-time visual–inertial odometry," *IEEE Transactions on Robotics*, vol. 33, no. 1, pp. 1–21, 2016.

[35] A. Kiamarzi, D. Rossi, and G. Tagliavini, "Qr-pulp: Streamlining qr decomposition for risc-v parallel ultra-low-power platforms," in *Proceedings of the 21st ACM International Conference on Computing Frontiers*, 2024, pp. 147–154.

[36] E. Cereda, M. Rusci, A. Giusti, and D. Palossi, "On-device self-supervised learning of visual perception tasks aboard hardware-limited nano-quadrotors," in *2024 IEEE International Conference on Robotics and Automation (ICRA)*, 2024, pp. 10 118–10 124.

[37] E. Anderson, Z. Bai, C. Bischof, L. S. Blackford, J. Demmel, J. Dongarra, J. Du Croz, A. Greenbaum, S. Hammarling, A. McKenney *et al.*, *LAPACK users' guide*. SIAM, 1999.

[38] J. Schur, "Über Potenzenreihen, die im Innern des Einheitskreises beschränkt sind." *Journal für die reine und angewandte Mathematik (Crelles Journal)*, vol. 1918, no. 148, pp. 122–145, 1918.

[39] M. Burri, J. Nikolic, P. Gohl, T. Schneider, J. Rehder, S. Omari, M. W. Achtelik, and R. Siegwart, "The euroc micro aerial vehicle datasets," *The International Journal of Robotics Research*, vol. 35, no. 10, pp. 1157–1163, 2016.

[40] Z. Zhang and D. Scaramuzza, "A tutorial on quantitative trajectory evaluation for visual (-inertial) odometry," in *2018 IEEE/RSJ International Conference on Intelligent Robots and Systems (IROS)*. IEEE, 2018, pp. 7244–7251.



**Jonas Kühne** (Member, IEEE) received the B.Sc. and M.Sc. degrees in electrical engineering and information technology from ETH Zürich, Zürich, Switzerland, in 2016 and 2018, respectively. Between 2019 and 2021, he worked for Agtatec AG, which is part of Assa Abloy. He is currently pursuing his Ph.D. degree with both the Integrated Systems Laboratory and the D-ITET Center for Project-Based Learning at ETH Zürich, Zürich, Switzerland.

His research interests include algorithm and hardware design for visual inertial odometry and SLAM on low-power embedded systems.

hardwar



**Christian Vogt** (Member, IEEE) received the M.Sc. degree and the Ph.D. in electrical engineering and information technology from ETH Zürich, Zürich, Switzerland, in 2013 and 2017, respectively. He is currently a post-doctoral researcher and lecturer at ETH Zürich, Zürich, Switzerland. His research work focuses on signal processing for low power applications, including field programmable gate arrays (FPGAs), IoT, wearables and autonomous unmanned vehicles.



**Michele Magno** (Senior Member, IEEE) received his master's and Ph.D. degrees in electronic engineering from the University of Bologna, Bologna, Italy, in 2004 and 2010, respectively.

Currently, he is a *Privatdozent* at ETH Zurich, Zurich, Switzerland, where he is the Head of the Project-Based Learning Center. He has collaborated with several universities and research centers, such as Mid University Sweden, where he is a Guest Full Professor. He has published more than 150 articles in international journals and conferences, in which he got multiple best paper and best poster awards. The key topics of his research are wireless sensor networks, wearable devices, machine learning at the edge, energy harvesting, power management techniques, and extended lifetime of battery-operated devices.



**Luca Benini** (Fellow, IEEE) received the Ph.D. degree in electrical engineering from Stanford University, Stanford, CA, USA, in 1997.

He holds the Chair of Digital Circuits and Systems at ETH Zurich, Zurich, Switzerland, and is a Full Professor at the University of Bologna, Bologna, Italy. His current research interests include energy-efficient computing systems' design from embedded to high performance.

Dr. Benini is a fellow of the ACM and a member of the Academia Europaea. He was a recipient of the 2016 IEEE CAS Mac Van Valkenburg Award and the 2023 McCluskey Award.